Targeted Radionuclide Therapy in Patient-Derived Xenografts Using ^{177}Lu-EB-RGD

Liang Zhao[1], Haojun Chen[2], Zhide Guo[3], Kaili Fu[1], Lanling Yao[2], Li Fu[4], Weixi Guo[5], Xuejun Wen[3], Orit Jacobson[6], Xianzhong Zhang[3], Long Sun[2], Hua Wu[2], Qin Lin[1], and Xiaoyuan Chen[6]

ABSTRACT

Currently, most patients with non–small cell lung cancer (NSCLC) are diagnosed in advanced stages with a poor five-year survival rate. Therefore, intensive research aimed at finding novel therapeutic strategies has been ongoing; experimental models that reliably emulate NSCLC disease are greatly needed to predict responses to novel therapeutics. Therefore, we developed patient-derived xenograft (PDX) models of NSCLC, which we then used to evaluate the therapeutic efficacy of ^{177}Lu-EB-RGD, a peptide-based radiopharmaceutical with improved pharmacokinetics that targets integrin $\alpha_v\beta_3$. In this study, three different groups of NSCLC-PDXs were successfully established, all of which maintained the same IHC and genetic characteristics of the human primary tumor. The two NSCLC-PDX groups with intense and low expression of integrin $\alpha_v\beta_3$ (denoted as $PDX_{\alpha v\beta 3+}$ and $PDX_{\alpha v\beta 3-}$) were chosen as the experimental models to evaluate the *in vivo* biological behavior of ^{177}Lu-EB-RGD. In SPECT imaging and biodistribution studies, ^{177}Lu-EB-RGD showed significantly higher accumulation in $PDX_{\alpha v\beta 3+}$ and $PDX_{\alpha v\beta 3-}$ models than its corresponding monomer ^{177}Lu-RGD. A single dose of 18.5 MBq ^{177}Lu-EB-RGD was enough to completely eradicate the tumors in $PDX_{\alpha v\beta 3+}$, with no sign of tumor recurrence during the observation period. Such treatment was also efficacious in $PDX_{\alpha v\beta 3-}$: a single dose of 29.6 MBq ^{177}Lu-EB-RGD led to a significant delay in tumor growth as compared with that in the control or ^{177}Lu-RGD group. The preclinical data from the use of this model suggest that ^{177}Lu-EB-RGD may be an effective treatment option for NSCLC and should be further evaluated in human trials.

Introduction

Lung cancer is the leading cause of cancer-related death worldwide; approximately 2 million new cases and 1.8 million deaths were reported in 2018 by Global Cancer Statistics 2018 (1). The two major forms of lung cancer are non–small cell lung cancer (NSCLC) and small cell lung cancer. NSCLC accounts for approximately 80% to 85% of lung cancers, and adenocarcinoma is the most common histologic subtype. Currently, most NSCLC patients are diagnosed in advanced stages with five-year survival rates of less than 10% (2). Chemotherapy based on platinum is the first-line treatment for NSCLC but only provides a modest survival benefit (3). Therefore, a better understanding of the molecular basis of the NSCLC and novel therapies is needed to significantly improve patient outcome.

The last decade has witnessed a paradigm shift from cytotoxic drugs to targeted therapy in medical oncology and pharmaceutical innovation. Inspired by breakthroughs in molecular and cellular biology, several novel synthesized chemical compounds and recombinant antibodies have been developed to selectively target oncogenic signaling pathways in NSCLC (4). Such targeted therapeutic agents show impressive clinical efficacy and often significantly prolong the overall survival of individuals with NSCLC. Inevitably, however, the treated tumors recur as resistance to these targeted therapies develops (5). More recently, immunotherapies such as PD-1/PD-L1 immune-checkpoint blockades (ICB) have shown promise, with their durable response in advanced NSCLC without driver oncogene mutations (6). However, the low objective response rate is the main obstruction to using ICBs more widely.

Targeted radionuclide therapy (TRT), a branch of radiotherapy, uses isotope-emitting charged particles after labeling with a targeting vector. A carrier molecule can seek special molecular or functional targets. Besides being utilized in the treatment of local tumors such as external radiotherapy, TRT can treat metastatic tumors through systemic administration (7). A unique feature of radionuclides is that they can exert the "cross-fire" effect, potentially destroying adjacent tumor cells (8). On January of 2018, ^{177}Lu-labeled dodecanetetraacetic acid tyrosine-3-octreotate (DOTATATE; trade name Lutathera) was approved by the FDA to treat patients with somatostatin receptor-positive gastroenteropancreatic neuroendocrine tumors (NET; ref. 9).

Patient-derived xenografts (PDX), obtained by direct implantation of tissue fragments into immunodeficient mice, are of particular interest because they retain the morphology, architecture, and molecular signatures of the corresponding parental tumor more closely than

[1]Department of Radiation Oncology, Xiamen Cancer Center, The First Affiliated Hospital of Xiamen University, Xiamen, China. [2]Department of Nuclear Medicine and Minnan PET Center, Xiamen Cancer Center, The First Affiliated Hospital of Xiamen University, Xiamen, China. [3]State Key Laboratory of Molecular Vaccinology and Molecular Diagnostics and Center for Molecular Imaging and Translational Medicine, School of Public Health, Xiamen University, Xiamen, China. [4]Department of Pathology, Xiamen Cancer Hospital, The First Affiliated Hospital of Xiamen University, Xiamen, China. [5]Department of Thoracic Surgery, Xiamen Cancer Center, The First Affiliated Hospital of Xiamen University, Xiamen, China. [6]Laboratory of Molecular Imaging and Nanomedicine, National Institute of Biomedical Imaging and Bioengineering, NIH, Bethesda, Maryland.

Note: Supplementary data for this article are available at Molecular Cancer Therapeutics Online (http://mct.aacrjournals.org/).

L. Zhao, H. Chen, and Z. Guo contributed equally to this work.

Corresponding Authors: Haojun Chen, Department of Nuclear Medicine and Minnan PET Center, Xiamen Cancer Center, The First Affiliated Hospital of Xiamen University, Xiamen 361003, China. Phone: 86-592-2137077; E-mail: leochen0821@foxmail.com; Qin Lin, Department of Radiation Oncology, Xiamen Cancer Center, The First Affiliated Hospital of Xiamen University, Xiamen 361003, China. Phone: 86-592-2139152; E-mail: linqin05@163.com; and Xiaoyuan Chen, Laboratory of Molecular Imaging and Nanomedicine, National Institute of Biomedical Imaging and Bioengineering, NIH, Bethesda, MD 20814. Phone: 1-3013267145; E-mail: shawn.chen@nih.gov

Mol Cancer Ther 2020;19:2034–43

doi: 10.1158/1535-7163.MCT-19-1098

is possible for *in vitro*–established cell lines. PDXs have been successfully investigated to identify specific determinants of therapeutic response and to predict the therapy response of individual tumors to chemotherapy and targeted therapy. However, the potential of PDXs to predict the response of NSCLC to TRT has not been investigated. This has important clinical implications for patients with advanced NSCLC, especially for those who are ineffective or resistant to platinum-based therapy or epidermal growth factor receptor–tyrosine kinase inhibitors. In the present study, we investigated the therapeutic efficacy of peptide-based TRT in PDXs derived from NSCLC. The Arg–Gly–Asp (RGD) peptide targets the integrin $\alpha_v ß_3$ receptor on the tumor cells and neovasculature, which is highly expressed in many cancers (10). Our previous investigation has demonstrated the positive expression of integrin $\alpha_v ß_3$ in patients with NSCLC and ^{68}Ga-labeled RGD peptide (^{68}Ga-NOTA-PRGD2) could be of use for lesion detection and help stage patients with NSCLC (11). In this research, RGD was chemically conjugated with an albumin-binding moiety–truncated Evans Blue (denoted as EB-RGD). The major feature was the inclusion of the EB-derived albumin-binding moiety that affected the pharmacokinetics in a positive manner to elevate tumor uptake and tumor residence time (12, 13). For TRT application, EB-RGD was labeled with ^{177}Lu, which emits β rays. Through this investigation, we aimed to investigate whether PDXs could reproduce the same characteristics of the corresponding parental NSCLC and explore whether the ^{177}Lu-EB-RGD could be used as a novel therapeutic approach in patients with advanced NSCLC.

Materials and Methods

PDX establishment

Patients' written informed consent was obtained, and the research protocol was approved by the Clinical Research Ethics Committee of the First Affiliated Hospital of Xiamen University (ID KYZ2017-001). All animal care and experimental procedures were reviewed and approved by the Animal Care and Use Committee of Xiamen University Laboratory Animal Center (ID XMULAC20170063). The tumor specimens were obtained from patients who underwent presurgical ^{18}F-FDG PET/CT. After surgical resection, NSCLC specimens were immediately placed in DMEM (cat. #C11995599BT, Gibco) supplemented with 2% antibiotics (penicillin and streptomycin) and transferred into the icebox.

Immunodeficient BALB/c nude mice were bred under sterile conditions in Xiamen University Laboratory Animal Center from founders originally obtained from Charles River Co., Ltd. To establish PDXs, a fresh tumor specimen was processed into approximately 30 mm^3 for implantation subcutaneously (s.c.) at the level of transscapular brown fat of 4 to 6 weeks BALB/c nude female mice within an average of 2 hours following the patient's surgery. Tumor growth was monitored at least twice weekly using calipers until it reached a maximal volume of 1,500 mm^3, after which the mouse was euthanized by cervical dislocation, and the tumor was removed. The tumor was minced with scissors, and tumor fragments were implanted in BALB/c nude mice; the remaining fragments were used for histopathologic analyses. For investigational purposes, PDXs were expanded in a higher number of mice to obtain statistically relevant results.

Radiochemistry

Cyclic-RGD peptide was purchased from C.S. Bio for research purpose. EB-RGD was synthesized as previously described (13). Details of synthetic procedures and characterization of chemical components are described in Supplementary Fig. S1. High-purity radionuclide ^{177}Lu was purchased from ITG in a solution of $^{177}LuCl_3$. For radiolabeling, 1.85 GBq of $^{177}LuCl_3$ was diluted using 4 mL of 0.05 M HCl. EB-RGD (100 μg) or RGD (100 μg) was dissolved in 1 mL of 0.25 M NH_4OAc (pH = 5.6), and subsequently added to the $^{177}LuCl_3$. The mixture was heated at 90°C for 30 minutes; a C_{18} column was used for purifying and a 0.22-μm filtration membrane was used to ensure sterility. Next, 1 mL ethanol of 60% volume fraction was injected into the product container through a C_{18} column and aseptic filtration membrane; further, 5 mL normal saline was added. The ethanol concentration in the solution was about 10% when the tail vein was injected. Analytical thin-layer chromatography (Bioscan) was used for radiochemical purity control. Moreover, we evaluated the ^{177}Lu-EB-RGD stability both *in vitro* and *in vivo*; the methodology for stability assays can be found in Supplementary Material.

SPECT imaging and biodistribution study in NSCLC-PDX models

Single-photon emission computer tomography (SPECT) was performed with the Mediso multi-pinhole camera; 18.5 MBq of ^{177}Lu-EB-RGD or ^{177}Lu-RGD were intravenously (i.v.) injected into NSCLC-PDXs ($n = 4$). Whole-body SPECT imaging was performed as described previously (12). The acquisition times were at 4, 24, 48, 72, and 96 hours postinjection (p.i.). Regions of interest of the tumor, liver, heart, and muscle were counted on the SPECT images to quantify the radioactive signals, which were recorded as blood-to-muscle (B/M), tumor-to-muscle (T/M), and liver-to-muscle (L/M) ratios.

In the biodistribution study, groups of NSCLC-PDXs were injected with the same batch (same specific activities) of 0.5 MBq ^{177}Lu-EB-RGD and were sacrificed at different times (4, 24, 48, and 72 hours p.i.; $n = 3$ for each time point, 12 mice for each group). The main organs and tumor were weighed and analyzed. The ^{177}Lu-RGD group biodistribution was performed for contrasting as well. Groups of NSCLC-PDXs were sacrificed at 24 hours p.i. ($n = 3$ for each group). The γ-counter (WIZARD 2480) was used for assaying radioactivity.

The *in vivo* distribution pattern of EB-RGD and RGD was further evaluated via dynamic PET scan (using ^{68}Ga-EB-RGD and ^{68}Ga-RGD as the PET tracer) in healthy BALB/C mice. The half-life of EB-RGD and RGD were calculated by drug and statistics software (DAS version 2.0). The methodology for the dynamic PET scan can be found in Supplementary Material.

In vivo therapy regimen

NSCLC-PDXs were used for *in vivo* therapy study when the tumor volume reached approximately 100 mm^3. NSCLC-PDXs were divided into four groups (9–10 mice/group): group A, 100 μL saline; group B, 29.6 MBq of ^{177}Lu-RGD; group C, 18.5 MBq of ^{177}Lu-EB-RGD; group D, 29.6 MBq of ^{177}Lu-EB-RGD (all drugs were injected through i.v.

Tumor volume and body weight were recorded each 2 days. The formula: (length × width × width)/2, was used to calculate tumor volume. Three days after the beginning of treatment, groups A–D ($n = 3$) from NSCLC-PDXs underwent ^{18}F-FDG PET (Inveon, Siemens) imaging. The ^{18}F-FDG PET imaging protocol was performed as previously described (14).

The endpoint criteria for mice were as follows: tumor volume >1,500 mm^3, weight loss >20%, or active tumor ulceration.

Histopathologic staining

Animal tumor specimens from each group were sectioned at day 14 after treatment. CD31 IHC was used to picture the endothelial cells.

The primary antibodies of this experiment were anti-mouse CD31 mAb (ab9498; Abcam), Ki-67-specific mAb (ab15580; Abcam), human integrin $\alpha_v\beta_3$ (ab7166; Abcam), and murine integrin $\alpha_v\beta_3$ (CD61, Novus Biologicals, SJ19-09). Using these markers, routine IHC staining was performed according to our previous protocol (13). The expression of integrin $\alpha_v\beta_3$ was further detected by Western blot analysis; the protocol can be found in Supplementary Material. A commercially available kit (Roche Applied Science) was for immunofluorescent TdT-mediated dUTP Nick-End Labeling (TUNEL) analysis. Hematoxylin and eosin (H&E) staining was procured by Univ-Bio Inc.

Statistical analysis

All quantitative data are expressed as mean ± SD. All statistical analyses were conducted by using SPSS 22.0 statistical analysis software (IBM). One-way analysis of variance and Student *t* test were used to compare means. A P value of < 0.05 was considered statistically significant.

Results

Radiolabeled compound preparation

Two radioligands with high affinity for integrin $\alpha_v\beta_3$ were prepared in this study—^{177}Lu-EB-RGD and ^{177}Lu-RGD—both of which had >95% radiochemical purity after purification. ^{177}Lu-RGD and ^{177}Lu-EB-RGD were radiolabeled at an average specific activity of 18.6 ± 4.7 and 55.85 ± 14.0 GBq/μmol, respectively.

Stability of ^{177}Lu-EB-RGD

^{177}Lu-EB-RGD was stable in mouse serum for up to 24 hours with no significant demetalation observed. *In vivo*, over 90% of the radioactivity was bound to the blood proteins and not extractable. The extracted radioactivity showed ^{177}Lu-EB-RGD with only a small amount of a more polar component appearing at 4 hours after i.v. injection.

NSCLC-PDX establishment and validation

Fragments of primary tumor tissues were collected from eight patients who underwent surgical resection, and the diagnosis of NSCLC was confirmed by histopathology. The small fragments of primary tumor tissues were subsequently implanted into eight groups of immunodeficient BALB/c nude mice for propagation. Finally, three different groups of NSCLC-PDXs were successfully established, all of which were derived from adenocarcinomas. The three groups had different clinical stages (1 stage IB, 1 stage IIA, and 1 stage IIIA), different degrees of lymph node involvement (1 N0, 1 N1, and 1 N3), and different degrees of integrin $\alpha_v\beta_3$ expression levels (1 intense, 1 moderate, and 1 low expression). No driver mutations were observed in any of the three groups. The latency times (time interval from implantation to presence of palpable tumor; range, 23.3–65.6 days after implantation) and tumor growth rate (Supplementary Fig. S2) varied in the three groups. The phenotype of each NSCLC patient is summarized in Supplementary Table S1. All these parameters were consistent between the NSCLC-PDXs and their corresponding primary NSCLC (Supplementary Table S2), confirming the unique nature of individual PDXs. The two NSCLC-PDX groups with intense and low integrin $\alpha_v\beta_3$ expression (denoted as $PDX_{\alpha v\beta 3+}$ and $PDX_{\alpha v\beta 3-}$) were chosen as the experimental models to evaluate the *in vivo* biological behavior of ^{177}Lu-EB-RGD. It is worth noting that integrin $\alpha_v\beta_3$ is expressed on both tumor cells and neovasculature. Although $PDX_{\alpha v\beta 3-}$ tumors have low expression of integrin $\alpha_v\beta_3$ on the tumor cells, they show high levels of murine vascular integrin expression (CD61, murine integrin $\alpha_v\beta_3$). The PET imaging and histopathology information from the two PDX groups and their parental tumors are presented in **Fig. 1**.

SPECT imaging and biodistributions of ^{177}Lu-EB-RGD in NSCLC-PDXs

Whole-body SPECT imaging studies were performed for exploring the *in vivo* behavior of ^{177}Lu-EB-RGD. Representative whole-body maximum intensity projections (MIP) of $PDX_{\alpha v\beta 3+}$ and $PDX_{\alpha v\beta 3-}$ are presented in **Fig. 2**.

SPECT imaging of ^{177}Lu-EB-RGD in $PDX_{\alpha v\beta 3+}$ is shown in **Fig. 2A**. High tumor-to-background ratio was observed at 4 hours p.i. (T/M: 7.34 ± 0.67), and elevated at 24 and 48h p.i., with tumor uptake peaking at 72 hours p.i. (T/M: 15.99 ± 5.42) and reducing slightly from 96 to 120 hours p.i. Blood ^{177}Lu-EB-RGD uptake was comparatively high at 1 hour p.i. (B/M: 4.31 ± 1.22), and decreased from 24 to 120 hours p.i. gradually. The kidneys also showed a ^{177}Lu signal, which gradually decreased from 24 to 120 hours p.i. As shown in **Fig. 2B**, ^{177}Lu-EB-RGD uptake in $PDX_{\alpha v\beta 3-}$ was significantly lower than that in $PDX_{\alpha v\beta 3+}$ at all time points. The T/M ratios in $PDX_{\alpha v\beta 3-}$ from 4 to 96 hours p.i were 4.18 ± 0.74, 5.17 ± 4.11, 6.97 ± 1.12, 6.62 ± 1.64, and 7.34 ± 0.67, respectively. ^{177}Lu-RGD SPECT imaging in both $PDX_{\alpha v\beta 3+}$ and $PDX_{\alpha v\beta 3-}$ was also performed for comparison (**Fig. 2A** and **B**). ^{177}Lu-RGD was shown to be cleared from the blood rapidly and showed a significantly low accumulation in both PDXs at 24 hours p.i.

The biodistributions of ^{177}Lu-EB-RGD in the two PDX groups were obtained at different time points p.i. (**Fig. 3**). The biodistribution results were generally in line with previous SPECT imaging studies. In the case of $PDX_{\alpha v\beta 3+}$ (**Fig. 3A**), ^{177}Lu-EB-RGD accumulated mainly in the blood (12.99 ± 1.54 %ID/g) at 4 hours p.i. Moreover, ^{177}Lu-EB-RGD uptake was also observed in the kidney (9.81 ± 1.83 %ID/g), liver (7.56 ± 4.89 %ID/g), and spleen (7.87 ± 1.95 %ID/g). Tumor uptake at this time was 10.75 ± 1.17 %ID/g. ^{177}Lu-EB-RGD in the blood, kidneys, liver, and spleen had decreased to 4.41 ± 0.45, 8.99 ± 0.99, 6.06 ± 0.65, and 5.61 ± 2.67 %ID/g at 24 hours p.i., respectively, whereas the tumor uptake had increased to 13.38 ± 1.04 %ID/g. ^{177}Lu-EB-RGD uptake in tumor had reached its peak (14.87 ± 6.71 %ID/g) at 48 hours p.i., whereas the uptake in blood (1.71 ± 0.35 %ID/g), kidneys (7.78 ± 1.58 %ID/g), liver (5.60 ± 0.75 %ID/g), and spleen (5.23 ± 1.04 %ID/g) had continued to decrease. At 72 hours p.i., ^{177}Lu-EB-RGD further clearance from all organs was observed. A similar *in vivo* distribution pattern was observed in $PDX_{\alpha v\beta 3-}$ (**Fig. 3B**), except for the significantly reduced tumor uptake at all time points tested (^{177}Lu-EB-RGD uptakes in $PDX_{\alpha v\beta 3-}$ from 4 to 72 hours p.i. were 4.89 ± 1.33, 6.25 ± 0.56, 6.47 ± 1.50, and 5.55 ± 2.05 %ID/g, respectively).

The ^{177}Lu-RGD biodistribution was also investigated for comparison (**Fig. 3C** and **D**). In accordance with the SPECT findings, ^{177}Lu-RGD demonstrated a much shorter blood half-life than ^{177}Lu-EB-RGD in both PDX groups. The blood uptake of ^{177}Lu-RGD was almost 15 times lower than ^{177}Lu-EB-RGD at 24 hours p.i. Therefore, ^{177}Lu-EB-RGD demonstrated a significantly higher tumor uptake in both $PDX_{\alpha v\beta 3+}$ (13.38 ± 1.04 vs. 2.59 ± 1.60 %ID/g) and $PDX_{\alpha v\beta 3-}$ (6.26 ± 0.56 vs. 1.56 ± 0.35 %ID/g). The promising high tumor uptake of ^{177}Lu-EB-RGD and prolonged tumor retention time resulted in high exposure to the radioactive isotope. The area under the curve calculated from the radioactivity accumulation in tumors over time is shown in Supplementary Fig. S3.

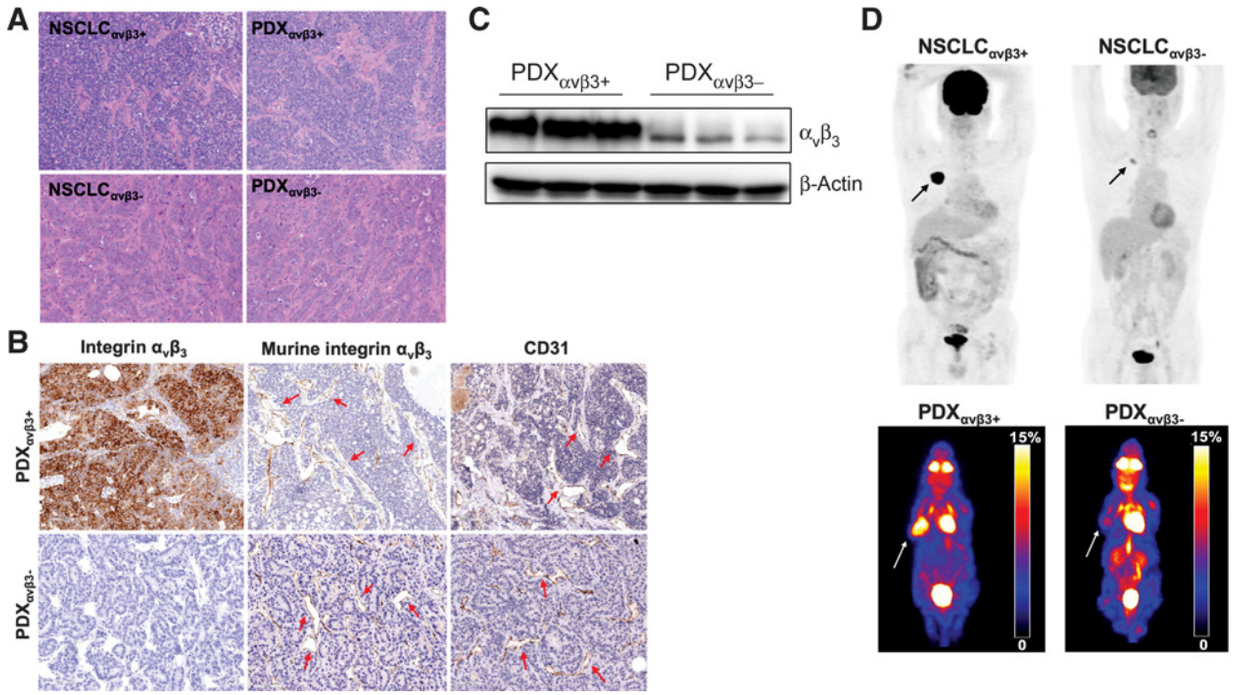

Figure 1.

Histopathology and PET imaging of PDX and parental tumors. **A,** H&E staining in human NSCLCs and corresponding PDXs; **B,** IHC staining of integrin $\alpha_v\beta_3$ expression and CD31 in human NSCLCs and corresponding PDXs (tumor vasculatures were indicated by arrows); **C,** the expression of integrin $\alpha_v\beta_3$ was detected by Western blot analysis; **D,** ^{18}F-FDG PET imaging in two patients with NSCLC and corresponding PDXs.

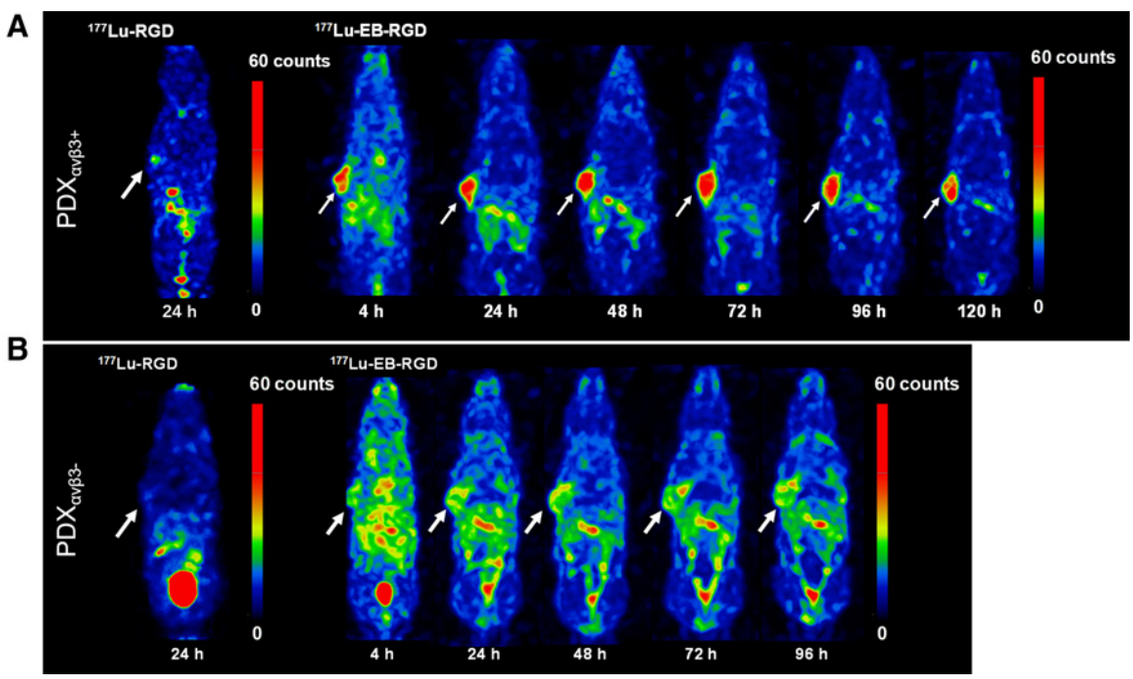

Figure 2.

MIP from SPECT imaging studies in PDXs. **A,** Projection SPECT images of mice in PDX$_{\alpha v\beta 3+}$ models at 24 hours after 18.5 MBq ^{177}Lu-RGD injection ($n = 4$) and at 4, 24, 48, 72, 96, and 120 hours after 18.5 MBq ^{177}Lu-EB-RGD injection ($n = 4$). **B,** Projection SPECT images of mice in PDX$_{\alpha v\beta 3-}$ models at 24 hours after 18.5 MBq ^{177}Lu-RGD injection ($n = 4$) and at 4, 24, 48, 72, and 96 hours after 18.5 MBq ^{177}Lu-EB-RGD injection ($n = 4$).

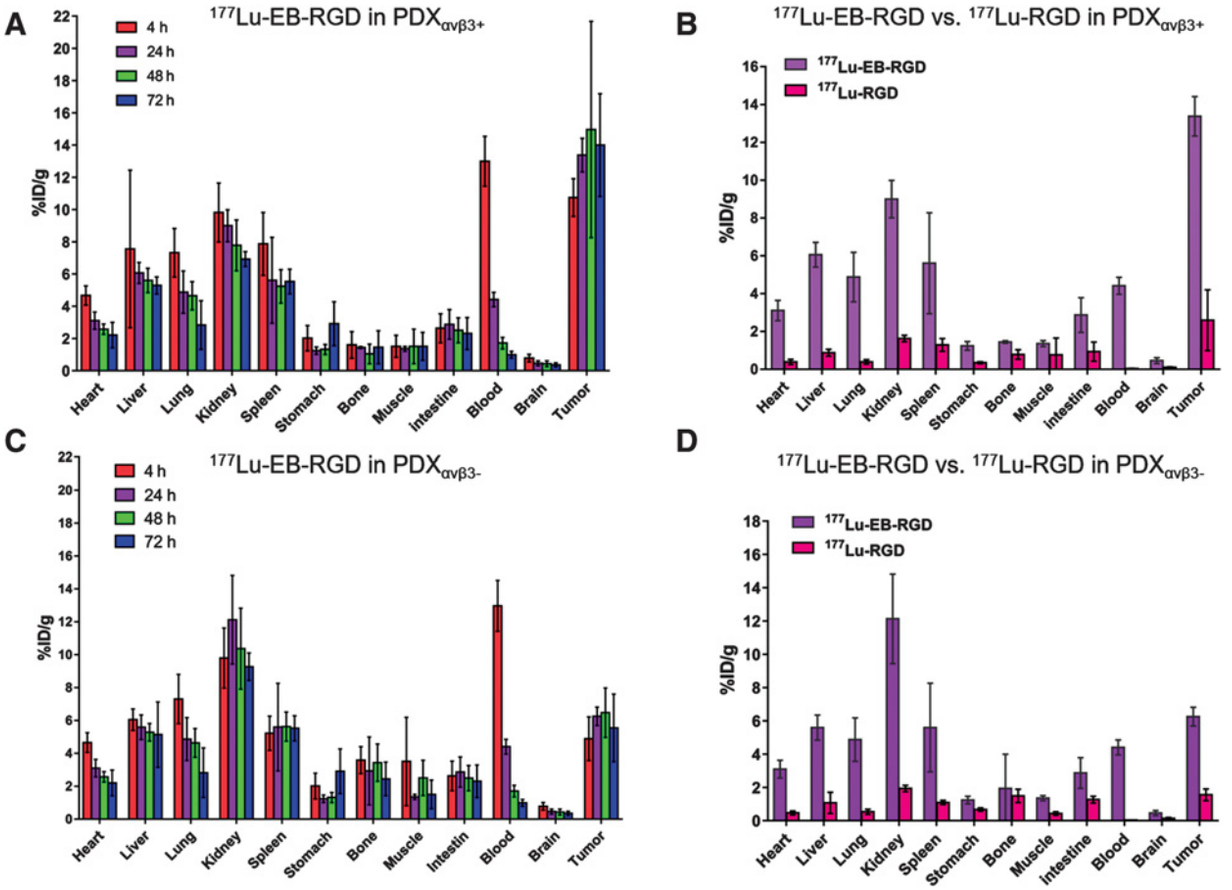

Figure 3.

Biodistribution of ^{177}Lu-EB-RGD in PDX groups. **A,** $PDX_{\alpha v\beta 3+}$ models at 4, 24, 48, and 72 hours after injection ($n = 3$). **B,** Comparison of ^{177}Lu-EB-RGD and ^{177}Lu-RGD in $PDX_{\alpha v\beta 3+}$ models at 24 hours after injection ($n = 3$/group). **C,** ^{177}Lu-EB-RGD in $PDX_{\alpha v\beta 3-}$ models at 4, 24, 48, and 72 hours after injection ($n = 3$/group). **D,** Comparison of ^{177}Lu-EB-RGD and ^{177}Lu-RGD in $PDX_{\alpha v\beta 3-}$ models at 24 hours after injection ($n = 3$/group).

Furthermore, pharmacokinetic parameters of EB-RGD and RGD were calculated by dynamic PET scan (Supplementary Fig. S4), which demonstrated that intravenously administered RGD was cleared from the circulation rapidly with a $t_{1/2}$ of 33.4 ± 0.9 minutes. The $t_{1/2}$ of EB-RGD was 167.8 ± 19.7 minutes, a 5-fold longer half-life than that of RGD.

^{177}Lu-EB-RGD demonstrates significant antitumoural radiotherapy efficacy in NSCLC-PDXs

To investigate whether ^{177}Lu-EB-RGD TRT would be efficacious in NSCLC-PDXs, the antitumoral radiotherapy efficacy of ^{177}Lu-EB-RGD was first evaluated in $PDX_{\alpha v\beta 3+}$ subjects, which were divided into four groups (A–D) and monitored for 50 days after treatment. **Figure 4A** showed therapy protocols along with the mice relative tumor volumes and body weight.

Transient weight loss was observed in this PDX, and mice regained their starting weight by the end of the study (**Fig. 4B**). Group A (saline) and group B (29.6 MBq of ^{177}Lu-RGD) showed rapid tumor growth. All PDXs in groups A and B had to be euthanized by day 36 because of excessive tumor volume (**Fig. 4C**, pink and purple lines). To evaluate the appropriate therapy dose of ^{177}Lu TRT, ^{177}Lu-EB-RGD was delivered in a radioactive dose of either 18.5 MBq (group C) or 29.6 MBq (group D). In groups C and D, significant inhibition of tumor growth could be seen (**Fig. 4C**). ^{77}Lu-EB-RGD and saline-treated groups showed significant difference in tumor volume starting from day 4 ($P = 0.007$), whereas the ^{177}Lu-EB-RGD and ^{177}Lu-RGD groups demonstrated significant difference starting from day 6 ($P = 0.001$). These differences increased over time; most tumors in the ^{177}Lu-EB-RGD therapy groups began to shrink from day 6 and completely disappeared at day 24. Although group D showed a faster tumor inhibition rate as compared with group C, all of the PDXs (9/9, 100%) in both groups finally showed a complete response (CR), with all of these CR maintaining for the duration of the 50 days study. Kaplan–Meier curves based on the protocol endpoints showed significant differences ($P < 0.001$) between groups A–B and groups C–D, but no significant difference was observed between groups C and D (**Fig. 4D**). Survival rates in the two ^{177}Lu-EB-RGD–treated groups were maintained at 100% up to day 50 after the initial treatment. Therefore, a therapy dose of 18.5 MBq ^{177}Lu-EB-RGD may be strong enough for tumor elimination in the PDXs with intense integrin $\alpha_v\beta_3$ expression.

During treatment, early therapeutic response was evaluated by ^{18}F-FDG PET at day 3 after treatment. Representative ^{18}F-FDG PET images of four therapy groups are presented in **Fig. 4E**. Compared with the saline control and ^{177}Lu-RGD-treated groups, significantly decreased ^{18}F-FDG uptake was observed in the ^{177}Lu-EB-RGD–

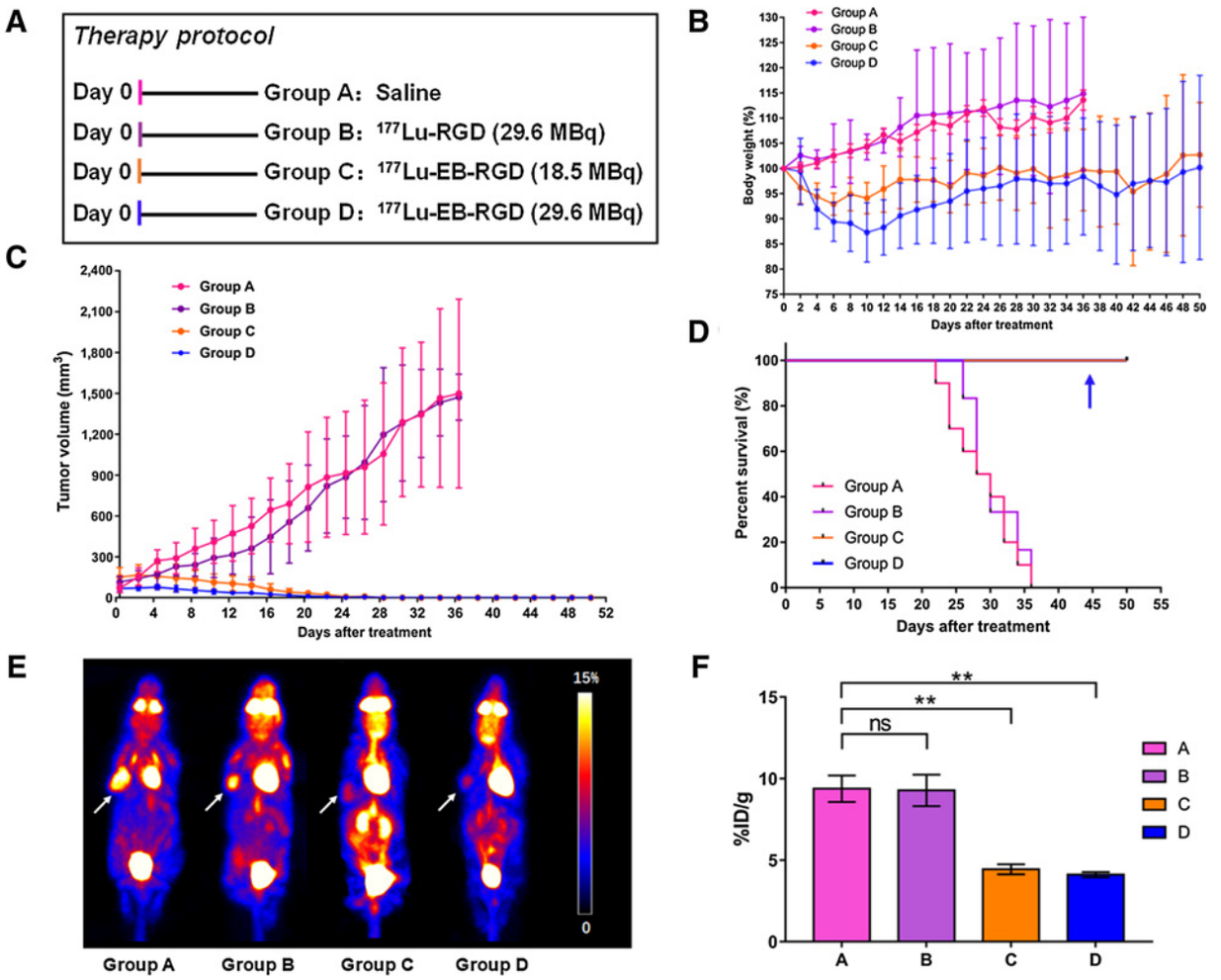

Figure 4.

Therapy protocol and outcomes in PDX$_{\alpha v\beta 3+}$ mice. **A,** Design of therapy protocol in PDX$_{\alpha v\beta 3+}$ models (n = 9 or 10 per group). **B,** Change in body weight after treatment. **C,** Change in tumor volume after treatment. **D,** Survival of mice after therapy (groups C and D were overlapped; group D was indicated by the blue arrow). **E,** Projection PET images of PDX$_{\alpha v\beta 3+}$ models injected with ^{18}F-FDG at 3 days after treatment. **F,** PET quantification of the images in E. **, $P < 0.01$.

treated groups (**Fig. 4F**), indicating reduced tumor metabolism following ^{177}Lu TRT.

We also tested the therapeutic efficacy of ^{177}Lu-EB-RGD in the NSCLC-PDXs with low expression (PDX$_{\alpha v\beta 3-}$), using the same therapy protocol among four groups (**Fig. 5A**). Once again, transient weight loss due to ^{177}Lu TRT was observed in these PDX$_{\alpha v\beta 3-}$, although the extent of weight loss was lower than that of PDX$_{\alpha v\beta 3+}$ (**Fig. 5B**). Tumor volumes in the two ^{177}Lu-EB-RGD–treated groups were similar to those in the control- and ^{177}Lu-RGD–treated groups up to day 8 after treatment, and then a minor tumor volume reduction was observed in both of the ^{177}Lu-EB-RGD–treated groups, which lasted for several days. However, tumor volumes in the ^{177}Lu-EB-RGD–treated groups increased once more from day 14 onward but grew at a slower rate than in the control- and ^{177}Lu-RGD–treated groups. In other words, ^{177}Lu-EB-RGD-TRT led to a delay in tumor growth in the PDX$_{\alpha v\beta 3-}$, rather than tumor shrinkage, as shown in PDX$_{\alpha v\beta 3+}$ (**Fig. 5C**).

Tumor biology evaluated by IHC

As shown in **Fig. 6**, groups C and D (18.5 and 29.6 MBq ^{177}Lu-EB-RGD) displayed a much lower extent of tumor vasculature than did groups A and B (saline and 29.6 MBq ^{177}Lu-RGD). Groups A and B demonstrated a relatively higher percentage of cells that stained positively for Ki-67, whereas groups C and D demonstrated reduced cell proliferation. Regarding TUNEL staining, both ^{177}Lu-EB-RGD groups showed considerably more cell apoptosis compared with groups A and B. H&E staining showed extensive necrotic areas for the ^{177}Lu-EB-RGD–treated groups, whereas tumors from the saline control and ^{177}Lu-RGD–treated groups only showed necrotic areas in the middle of the tumor. To further test the possible toxicity effects of ^{177}Lu-EB-RGD, pathologic examination of H&E staining of selected noncancerous organs was performed, which revealed no obvious differences between the ^{177}Lu-treated and control groups (Supplementary Fig. S5).

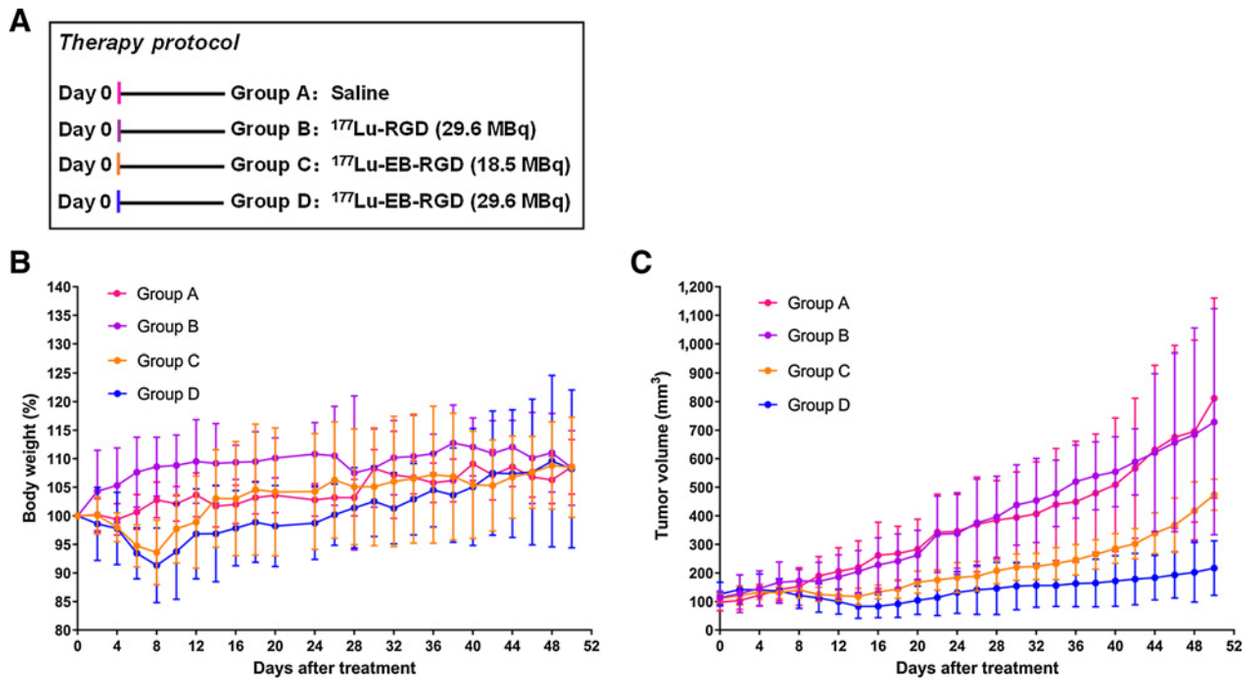

Figure 5.
Therapy protocol and outcomes in $PDX_{\alpha v\beta 3-}$ mice. **A,** Design of therapy protocol in the NSCLC-PDXs with low integrin expression ($PDX_{\alpha v\beta 3-}$). **B,** Change in body weight after treatment. **C,** Change in tumor volume after treatment.

IHC results in the $PDX_{\alpha v\beta 3-}$ groups were similar to those in the $PDX_{\alpha v\beta 3+}$ groups, except that fewer necrotic areas of $PDX_{\alpha v\beta 3-}$ were observed in ^{177}Lu-EB-RGD–treated groups as compared with those in $PDX_{\alpha v\beta 3+}$ (Supplementary Fig. S6).

Discussion

Current chemotherapy regimens have unsatisfactory results in most advanced NSCLC. Targeted therapies and immunotherapies represent two of the most researched types of therapy under current

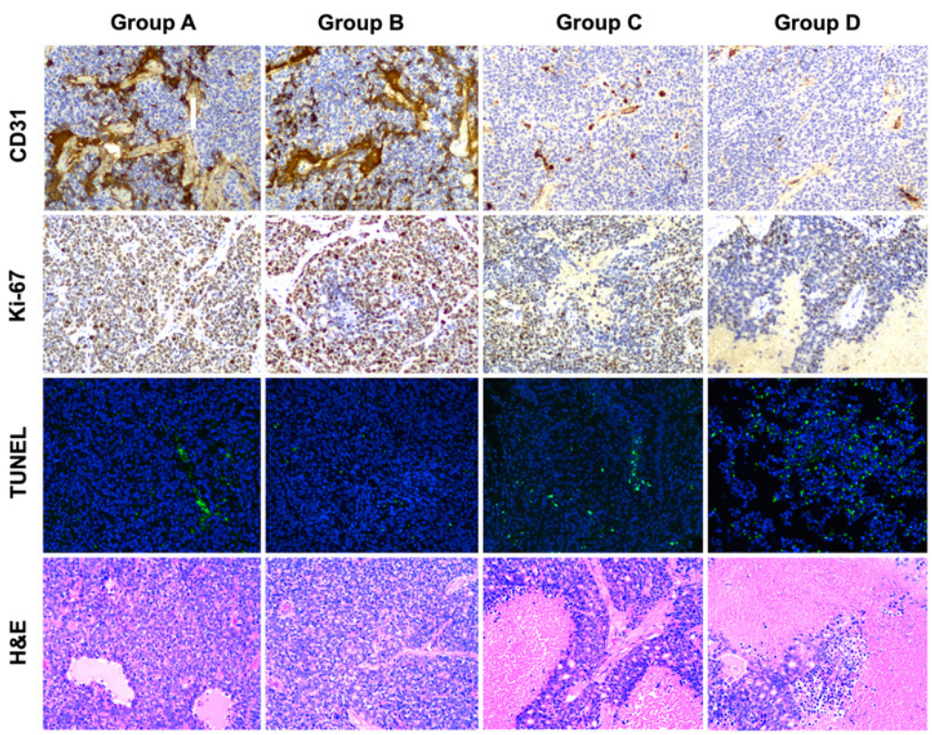

Figure 6.
IHC staining of excised tumors for CD31, Ki-67, TUNEL, and H&E after treatment with saline (group A), 29.6 MBq of ^{177}Lu-RGD (group B), 18.5 MBq of ^{177}Lu-EB-RGD (group C), and 29.6 MBq of ^{177}Lu-EB-RGD (group D) in $PDX_{\alpha v\beta 3+}$ models.

investigation for the treatment of NSCLC (4). However, over 80% of patients with advanced NSCLC do not have oncogenic driver biomarker status, and resistance is inevitable (4). Immunotherapy, especially ICB therapy, provides the hope that long-term survival is achievable in a subset of patients, but ICB therapy could only benefit a small population of patients (15). It is imperative, therefore, to develop novel therapeutic strategies and to optimize selection of patients, identifying early those who could benefit from available treatments.

Mouse tumor models are the most valuable tool for preclinical evaluation of novel therapeutic strategies in cancer (16). However, some drugs that show therapeutic efficacy against human tumor xenografts have often failed to show activity in human clinical trials (17, 18), resulting in an imperfect correlation between preclinical and clinical results in terms of therapeutic efficacy. Recently, some studies have demonstrated that PDXs have great potential in drug development studies because they reliably reproduce the patient's parental tumor for both IHC markers and genetic alterations as well as for evaluating the response to the corresponding therapeutic regimens. Moreover, PDXs accurately reproduce the heterogeneity of human cancers and maintain at least some aspects of the human microenvironment; therefore, they represent a promising preclinical model for studies of tumor heterogeneity and tumor–microenvironment studies (19, 20). As such, we investigated the establishment of PDXs from NSCLC as a source of therapeutically relevant information. As expected, our results demonstrated that PDXs derived from NSCLC can maintain the same IHC and genetic characterization of the human primary tumor, confirming the robustness of this model to test the efficacy of new treatments for NSCLC. Moreover, in our experience, growth features of PDX (such as latency time and tumor growth rate) reach stability after 3 to 4 passages in mice; it is therefore advisable to carry out drug efficacy evaluation with PDXs that have reached a certain stability in their growth characteristics.

We have further confirmed the robustness of PDXs by using PET imaging, which showed concordant uptake of ^{18}F-FDG between primary NSCLC and corresponding PDXs. Interestingly, lower ^{18}F-FDG uptake was observed in PDXs with lower integrin $\alpha_v\beta_3$ expression. This may be partially explained by the finding that both integrin $\alpha_v\beta_3$ expression and ^{18}F-FDG uptake are correlated with tumor aggressiveness and prognosis in NSCLC (21). However, it cannot be concluded that ^{18}F-FDG provides information similar to that of an RGD-based tracer, because both tracers have completely different pharmacodynamic properties. In a previous study (22), Beer and colleagues compared ^{18}F-RGD and ^{18}F-FDG uptake on PET in primary and metastatic tumor lesions in patients with cancer and found no substantial correlation between ^{18}F-RGD and ^{18}F-FDG uptake, suggesting that $\alpha_v\beta_3$ expression and glucose metabolism are not closely linked in malignant lesions.

TRT is the use of radioisotopes to deliver ionization energy to tumor cells (8). TRT is particularly useful in cases of metastatic disease where conventional treatments are no longer effective (7, 23). According to previous clinical trials in NETs and castration-resistant prostate cancer (CRPC), ^{177}Lu TRT results in high responses, a low toxicity profile, and improves overall survival (23, 24). As such, TRT may also provide a novel strategy for the treatment of advanced NSCLC. Although several preclinical studies have demonstrated a significant antitumor efficacy of TRT in lung cancer mouse models (4), no clinical trial until now has provided a clue as to whether this approach holds promise or not. In our present study, we chose RGD peptide as the TRT vector for targeting the integrin $\alpha_v\beta_3$ receptor, which has been validated to be overexpressed in NSCLC and to have a crucial role in tumor angiogenesis (11). More importantly, the pharmacokinetics of the targeting vector RGD were further improved by conjugation of RGD with an albumin-binding moiety, the truncated EB. The reversible binding of EB to albumin has been well documented, with a stoichiometry of 8–14 dye molecules per molecule of albumin (25). In our previous study (13), we demonstrated that albumin can serve as a pool and allow the slow release of EB-RGD from albumin. The slow release of the drug over time would allow continual uptake at the biological target (integrin $\alpha_v\beta_3$ on tumor cells and vasculature). Furthermore, internalization assays in our previous study have found that most of the EB-RGD was internalized into tumor cells (due to $\alpha_v\beta_3$ receptor–mediated internalization), whereas albumin was not internalized in the presence of EB-RGD.

Improved pharmacokinetics of EB-RGD, demonstrated by both a longer half-life and higher retention in the blood pool, resulted in significantly higher accumulation of ^{177}Lu-EB-RGD and enhanced tumor-to-background ratios as shown in SPECT imaging and biodistribution studies. The antitumor efficacy of ^{177}Lu-EB-RGD in NSCLC-PDXs is also quite impressive: a therapeutic dose of 18.5 MBq ^{177}Lu-EB-RGD was enough to completely eradicate the NSCLC-PDXs with high integrin $\alpha_v\beta_3$ expression, with no sign of tumor recurrence during the observation period. Considering integrin $\alpha_v\beta_3$ is expressed on both tumor cells and neovasculature, ^{177}Lu-EB-RGD was able to target both tumor cells and tumor vasculature, as confirmed by the reduced expression of CD31 (a vascularization marker) and Ki-67 (a proliferation marker) after treatment.

Such TRT treatment was also efficacious even in the NSCLC-PDXs with low integrin $\alpha_v\beta_3$ expression; a therapeutic dose of 29.6 MBq ^{177}Lu-EB-RGD led to a significant delay in tumor growth as compared with control or ^{177}Lu-RGD monomer group. The modest therapeutic effect observed in this PDX may be due to the following reason: the tumor uptake of ^{177}Lu-EB-RGD can be divided into three portions, the expression of integrin $\alpha_v\beta_3$ on tumor cells and on neovasculature, as well as the reinforced vascular permeability and retention (EPR) effect. Although $PDX_{\alpha v\beta 3-}$ models have low expression of integrin $\alpha_v\beta_3$ within tumor cells, they exhibit high levels of murine vascular integrin $\alpha_v\beta_3$ expression (as confirmed by CD61 IHC staining). From the biodistribution study, ^{177}Lu-EB-RGD uptake in $PDX_{\alpha v\beta 3-}$ was about half that of $PDX_{\alpha v\beta 3+}$ tumor uptake (13.38 %ID/g vs. 6.26 %ID/g), which means 50% of tumor uptake may have been due to uptake by the neovasculature and EPR effect. The remaining 50% of ^{177}Lu-EB-RGD uptake in tumor could explain the observed therapeutic effect on PDX tumors with low integrin expression. Furthermore, we could also observe the reduced expression of CD31 in the $PDX_{\alpha v\beta 3-}$ tumors, suggesting that the modest therapeutic effect is partly due to the damage to the tumor vasculature.

In future clinical translation, ^{68}Ga/^{177}Lu-RGD theranostics could enable a highly personalized approach using ^{68}Ga-RGD PET/CT to noninvasively image and quantify integrin $\alpha_v\beta_3$ expression, and thereby select patients most likely to benefit from treatment. ^{68}Ga-RGD PET/CT can also be used to evaluate the response to therapy after ^{177}Lu-EB-RGD treatment; further therapy cycles can be cancelled if there is no or low uptake on posttreatment PET imaging (indicative of a complete or partial response). The principles and expertise required in RGD-based NSCLC theranostics broadly parallel those using ^{68}Ga/^{177}Lu–labeled DOTATATE for metastatic NETs (26, 27) or PSMA for metastatic CRPC (24, 28). However, based on previous trials using peptide receptor radionuclide therapy or peptide radioligand therapy, three to four cycles of ^{177}Lu-DOTATATE/^{177}Lu-PSMA are usually required for an entire treatment paradigm,

and each cycle requires a dose of at least 1.85–7.4 GBq of ^{177}Lu, resulting in a total dosage of 7.4–29.6 GBq ^{177}Lu (26, 29–31). Such a huge radiation dosage may result in treatment-related toxic effects on normal organs, such as salivary gland dysfunction, loss of kidney function, and hematological toxicity. However, according to our experience using ^{177}Lu-EB-TATE or ^{177}Lu-EB-PSMA (32, 33), a single dose of 1.85–3.70 GBq ^{177}Lu provides comparable therapeutic efficacy due to the enhanced tumor accumulation and prolonged retention of such EB derivatives. Unexpectedly, a single imaging dose (0.67–0.8 GBq) of ^{177}Lu-EB-TATE/^{177}Lu-EB-PSMA provides some therapeutic efficacy in some patients with NETs or CRPCs. The approximately 6-fold lower dosage of ^{177}Lu and reduced dosing frequency would greatly decrease the potential side effects and increase patient compliance.

Besides the pharmacokinetics of radiotherapeutic agents, barriers to the success of TRT include the heterogeneous expression of molecular markers on cancer cells and poor vasculature of the tumor, which would prevent delivery of the agents (34). In addition, the biological response to TRT of individual cells within a tumor may vary depending on cell-specific radiosensitivity to the radiotherapeutic agent (35). Other variables that are important in TRT include the biological effectiveness of the emitted particles, dose rate and the induction of bystander responses (36). These properties of TRT may be exploitable in rationally designed combination protocols that aim to complement the strengths of TRT with other therapeutics and take into consideration optimal timing and sequencing. In our latest study, the combination of TRT (^{177}Lu-EB-RGD) and immune-checkpoint inhibitors (anti–PD-L1 antibodies) in MC38 colon cancer xenografts enhanced mice survival significantly as compared with that of TRT or immunotherapy alone (12). This combination may represent a promising approach for metastatic tumors in which TRT can be used. Therefore, a concentrated effort is needed to shift research from preclinical studies to randomized trials of combination treatments if the potential of TRT is to be fully exploited. The integration of TRT into first-line therapy, rather than as a treatment for end-stage disease (which has been the norm to date) is predicted to be beneficial in the future.

In conclusion, we have designed a theranostic agent, based on an RGD peptide, that targets integrin $\alpha_v\beta_3$-expressing NSCLC and demonstrates improved pharmacokinetics. Using the β-emitting radionuclide ^{177}Lu, we obtain improved contrast for SPECT imaging and effective TRT for NSCLC-PDXs. Furthermore, our PDX models maintain the same IHC and genetic characteristics of the human primary tumor. These preclinical data suggest that ^{177}Lu-EB-RGD may be an effective treatment option for NSCLC that should be further evaluated in human trials.

Disclosure of Potential Conflicts of Interest

O. Jacobson reports a patent 20190084931 pending, issued, licensed, and with royalties paid from Molecular Targeting Technologies. X. Chen reports a patent 20190084931 pending, issued, licensed, and with royalties paid from Molecular Targeting Technologies, Inc. No potential conflicts of interest were disclosed by the other authors.

Authors' Contributions

L. Zhao: Conceptualization, investigation, and writing–original draft. **H. Chen:** Conceptualization, data curation, funding acquisition, project administration, writing–review, and editing. **Z. Guo:** Resources, software, supervision, and methodology. **K. Fu:** Software, investigation, and methodology. **L. Yao:** Investigation and methodology. **L. Fu:** Resources. **W. Guo:** Resources. **X. Wen:** Software and methodology. **O. Jacobson:** Data curation and methodology. **X. Zhang:** Data curation and methodology. **L. Sun:** Data curation and methodology. **H. Wu:** Data curation and methodology. **Q. Lin:** Conceptualization, funding acquisition, writing–review, and editing. **X. Chen:** Conceptualization, supervision, funding acquisition, writing–review, and editing.

Acknowledgments

This study was funded by the National Natural Science Foundation of China (Grant number 81772893, to Q. Lin; and 81701736, to H. Chen), Fujian Middle-aged Backbone Talents Program (2017-ZQN-82, to H. Chen), and the Intramural Research Program, National Institute of Biomedical Imaging and Bioengineering, NIH (to X. Chen).

The costs of publication of this article were defrayed in part by the payment of page charges. This article must therefore be hereby marked *advertisement* in accordance with 18 U.S.C. Section 1734 solely to indicate this fact.

Received November 23, 2019; revised May 1, 2020; accepted August 7, 2020; published first August 26, 2020.

References

1. Bray F, Ferlay J, Soerjomataram I, Siegel RL, Torre LA, Jemal A. Global cancer statistics 2018: GLOBOCAN estimates of incidence and mortality worldwide for 36 cancers in 185 countries. CA Cancer J Clin 2018;68:394–424.
2. Ettinger DS, Akerley W, Bepler G, Blum MG, Chang A, Cheney RT, et al. Non-small cell lung cancer. J Natl Compr Canc Netw 2010;8:740–801.
3. Schiller JH, Harrington D, Belani CP, Langer C, Sandler A, Krook J, et al. Comparison of four chemotherapy regimens for advanced non-small-cell lung cancer. N Engl J Med 2002;346:92–8.
4. Naylor EC, Desani JK, Chung PK. Targeted therapy and immunotherapy for lung cancer. Surg Oncol Clin N Am 2016;25:601–9.
5. Cortot AB, Janne PA. Molecular mechanisms of resistance in epidermal growth factor receptor-mutant lung adenocarcinomas. Eur Respir Rev 2014;23:356–66.
6. Mok TSK, Wu Yi-L, Kudaba I, Kowalski DM, Cho BC, Turna HZ, et al. Pembrolizumab versus chemotherapy for previously untreated, PD-L1-expressing, locally advanced or metastatic non-small-cell lung cancer (KEYNOTE-042): a randomised, open-label, controlled, phase 3 trial. Lancet 2019;393:1819–30.
7. Iikuni S, Ono M, Watanabe H, Shimizu Y, Sano K, Saji H. Cancer radiotheranostics targeting carbonic anhydrase-IX with (111)In- and (90)Y-labeled ureidosulfonamide scaffold for SPECT imaging and radionuclide-based therapy. Theranostics 2018;8:2992–3006.
8. Pouget J-P, Navarro-Teulon I, Bardiès M, Chouin N, Cartron G, Pèlegrin A, et al. Clinical radioimmunotherapy–the role of radiobiology. Nat Rev Clin Oncol 2011;8:720–34.
9. FDA approves Lutathera for GEP NET therapy. J Nucl Med 2018;59:9N.
10. Chen H, Niu G, Wu H, Chen X. Clinical application of radiolabeled RGD peptides for PET imaging of integrin alphavbeta3. Theranostics 2016;6:78–92.
11. Zheng K, Liang N, Zhang J, Lang L, Zhang W, Li S, et al. 68Ga-NOTA-PRGD2 PET/CT for integrin imaging in patients with lung cancer. J Nucl Med 2015;56:1823–7.
12. Chen H, Zhao L, Fu K, Lin Q, Wen X, Jacobson O, et al. Integrin alphavbeta3-targeted radionuclide therapy combined with immune checkpoint blockade immunotherapy synergistically enhances anti-tumor efficacy. Theranostics 2019;9:7948–60.
13. Chen H, Jacobson O, Niu G, Weiss ID, Kiesewetter DO, Liu Yi, et al. Novel "Add-On" molecule based on Evans blue confers superior pharmacokinetics and transforms drugs to theranostic agents. J Nucl Med 2017;58:590–7.
14. Wu H, Chen H, Pan D, Ma Y, Liang S, Wan Y, et al. Imaging integrin alphavbeta 3 and NRP-1 positive gliomas with a novel fluorine-18 labeled RGD-ATWLPPR heterodimeric peptide probe. Mol Imaging Biol 2014;16:781–92.
15. Osmani L, Askin F, Gabrielson E, Li QK. Current WHO guidelines and the critical role of immunohistochemical markers in the subclassification of non-small cell lung carcinoma (NSCLC): moving from targeted therapy to immunotherapy. Semin Cancer Biol 2018;52:103–9.

16. Chow LQ, Eckhardt SG. Sunitinib: from rational design to clinical efficacy. J Clin Oncol 2007;25:884–96.
17. Burchill SA. What do, can and should we learn from models to evaluate potential anticancer agents? Future Oncol 2006;2:201–11.
18. Voskoglou-Nomikos T, Pater JL, Seymour L. Clinical predictive value of the in vitro cell line, human xenograft, and mouse allograft preclinical cancer models. Clin Cancer Res 2003;9:4227–39.
19. Blomme A, Van Simaeys G, Doumont G, Costanza B, Bellier J, Otaka Y, et al. Murine stroma adopts a human-like metabolic phenotype in the PDX model of colorectal cancer and liver metastases. Oncogene 2018;37:1237–50.
20. DeRose YS, Wang G, Lin Yi-C, Bernard PS, Buys SS, Ebbert MTW, et al. Tumor grafts derived from women with breast cancer authentically reflect tumor pathology, growth, metastasis and disease outcomes. Nat Med 2011; 17:1514–20.
21. Higashi K, Ito K, Hiramatsu Y, Ishikawa T, Sakuma T, Matsunari I, et al. 18F-FDG uptake by primary tumor as a predictor of intratumoral lymphatic vessel invasion and lymph node involvement in non-small cell lung cancer: analysis of a multicenter study. J Nucl Med 2005;46:267–73.
22. Beer AJ, Lorenzen S, Metz S, Herrmann K, Watzlowik P, Wester H-J, et al. Comparison of integrin alphaVbeta3 expression and glucose metabolism in primary and metastatic lesions in cancer patients: a PET study using 18F-galacto-RGD and 18F-FDG. J Nucl Med 2008;49:22–9.
23. Kessel K, Seifert R, Schäfers M, Weckesser M, Schlack K, Boegemann M, et al. Second line chemotherapy and visceral metastases are associated with poor survival in patients with mCRPC receiving (177)Lu-PSMA-617. Theranostics 2019;9:4841–8.
24. Hofman MS, Violet J, Hicks RJ, Ferdinandus J, Thang SP, Akhurst T, et al. [(177)Lu]-PSMA-617 radionuclide treatment in patients with metastatic castration-resistant prostate cancer (LuPSMA trial): a single-centre, single-arm, phase 2 study. Lancet Oncol 2018;19:825–33.
25. Lindner V, Heinle H. Binding properties of circulating Evans blue in rabbits as determined by disc electrophoresis. Atherosclerosis 1982;43:417–22.
26. Wolf KI, Jha A, van Berkel A, Wild D, Janssen I, Millo CM, et al. Eruption of metastatic paraganglioma after successful therapy with (177)Lu/(90)Y-DOTATOC and (177)Lu-DOTATATE. Nucl Med Mol Imaging 2019;53: 223–30.
27. Waldmann CM, Stuparu AD, van Dam RM, Slavik R. The search for an alternative to [(68)Ga]Ga-DOTA-TATE in neuroendocrine tumor theranostics: current state of (18)F-labeled somatostatin analog development. Theranostics 2019;9:1336–47.
28. Lindström E, Velikyan I, Regula N, Alhuseinalkhudhur A, Sundin A, Sörensen J, et al. Regularized reconstruction of digital time-of-flight (68)Ga-PSMA-11 PET/CT for the detection of recurrent disease in prostate cancer patients. Theranostics 2019;9:3476–84.
29. Roll W, Bode A, Weckesser M, Bögemann M, Rahbar K. Excellent response to 177Lu-PSMA-617 radioligand therapy in a patient with advanced metastatic castration resistant prostate cancer evaluated by 68Ga-PSMA PET/CT. Clin Nucl Med 2017;42:152–3.
30. Heinzel A, Boghos D, Mottaghy FM, Gaertner F, Essler M, von Mallek D, et al. (68)Ga-PSMA PET/CT for monitoring response to (177)Lu-PSMA-617 radioligand therapy in patients with metastatic castration-resistant prostate cancer. Eur J Nucl Med Mol Imaging 2019;46:1054–62.
31. Grubmüller B, Senn D, Kramer G, Baltzer P, D'Andrea D, Grubmüller KH, et al. Response assessment using (68)Ga-PSMA ligand PET in patients undergoing (177)Lu-PSMA radioligand therapy for metastatic castration-resistant prostate cancer. Eur J Nucl Med Mol Imaging 2019;46:1063–72.
32. Wang H, Cheng Y, Zhang J, Zang J, Li H, Liu Q, et al. Response to single low-dose (177)Lu-DOTA-EB-TATE treatment in patients with advanced neuroendocrine neoplasm: a prospective pilot study. Theranostics 2018;8:3308–16.
33. Zang J, Fan X, Wang H, Liu Q, Wang J, Li H, et al. First-in-human study of (177)Lu-EB-PSMA-617 in patients with metastatic castration-resistant prostate cancer. Eur J Nucl Med Mol Imaging 2019;46:148–58.
34. Gill MR, Falzone N, Du Y, Vallis KA. Targeted radionuclide therapy in combined-modality regimens. Lancet Oncol 2017;18:e414–23.
35. Rajon D, Bolch WE, Howell RW. Survival of tumor and normal cells upon targeting with electron-emitting radionuclides. Med Phys 2013;40:014101.
36. Prise KM, Folkard M, Michael BD. Bystander responses induced by low LET radiation. Oncogene 2003;22:7043–9.